From $CdPb_8(SeO_3)_4Br_{10}$ to $Pb_3(TeO_3)Br_4$: the first tellurite bromide exhibiting an SHG response and mid-IR transparency

Peng-Fei Li[a,b], Chun-Li Hu,[a] Bing-Xuan Li,[a] Jiang-Gao Mao[a,b], Fang Kong[*,a,b]

[a] State Key Laboratory of Structural Chemistry, Fujian Institute of Research on the Structure of Matter, Chinese Academy of Sciences, Fuzhou 350002, P. R. China.

[b] University of Chinese Academy of Sciences, Beijing 100049, P. R. China.

[*]Corresponding Authors: kongfang@fjirsm.ac.cn

Supporting Information

Experimental Section

Reagents and Instruments

All the chemicals were obtained from commercial sources and used without further purification: SeO_2 (Adamas-beta, 99.999%), CdO (Adamas-beta, 99.0%+), TeO_2 (Adamas-beta, 99.99%), $PbBr_2$ (Adamas-beta, 99.9%) and HBr (Adamas-beta, 48%).

Powder X-ray diffraction (PXRD) patterns of the two compounds were collected on the Miniflex 600 powder X-ray diffractometer using Cu Kα radiation (λ = 1.54186 Å) at room temperature in the angular range of 2θ = 10-70° with a scan step size of 0.02°.

Microprobe elemental analysis was carried out with the aid of a field-emission scanning electron microscope (JSM6700F) outfitted with an energy-dispersive X-ray spectroscope (Oxford INCA).

IR spectra were carried out on a Magna 750 FT-IR spectrometer using air as background in the range of 4000–400 cm^{-1} with a resolution of 2 cm^{-1} at room temperature. The samples used were polycrystalline powders of $CdPb_8(SeO_3)_4Br_{10}$ and $Pb_3(TeO_3)Br_4$.

The UV-vis-NIR spectra were obtained at 2000–200 nm by a PerkinElmer Lambda 900 spectrophotometer using $BaSO_4$ as the reference, and the reflection spectra were converted into an absorption spectrum using the Kubelka-Munk function. Absorption data was calculated from the diffuse reflection data by the Kubelka-Munk function: $\alpha/S = (1-R)^2/2R$, where α and S represent the absorption coefficient and the scattering coefficient, respectively[1]. The band gap value can be given by extrapolating the absorption edge to the baseline in the α/S vs. energy graph.

Thermogravimetric analyses (TGA) were measured by Netzsch STA 499C installation. The samples about 3.0-5.0 mg were placed in alumina crucibles and heated in 20-1200 °C at a rate of 15 °C/min under N_2 atmosphere.

Powder SHG measurements were conducted using a modified method of Kurtz and Perry [2]. Irradiation laser (λ = 1064 nm) is generated by a Nd:YAG solid-state laser equipped with a Q switch. The pure crystal samples of $Pb_3(TeO_3)Br_4$ was sieved according to 150−210 μm particle

size range. KH_2PO_4 (KDP) samples in the same size range were also be prepared and used as reference. The oscilloscope traces of SHG signals for $Pb_3(TeO_3)Br_4$ and KDP samples in the particle size range (150−210 μm) were recorded.

The LIDT measurements of the $Pb_3(TeO_3)Br_4$ crystal samples was performed by a Q-switched pulsed laser. The particle size range of the tested sample was 150−210 μm, the laser wavelength was 1064 nm, the pulse duration was 10 ns, the pulse frequency was 1 Hz, and the laser spot area focused on the sample was 1.54 mm^2. The energy of the laser emission was gradually increased during the measurement, and the LIDT of the sample was determined when it turned black under the laser.

Single-crystal X-ray diffraction data of $Pb_3(TeO_3)Br_4$ was obtained on Agilent Technologies SuperNova dual-wavelength CCD diffractometer with a graphite-monochromated Mo Kα radiation (λ = 0.71073 Å) at room temperature. Data reduction and cell refinement and were performed with *CrysAlisPro*. The structure was solved by the direct methods and refined by full-matrix least-squares fitting on F^2 using *Olex2* crystallographic software package[3, 4]. All the atoms were refined with anisotropic thermal parameters and finally converged for $F_0^2 \geq 2\sigma(F_0^2)$. The structural data were also checked for possible missing symmetry with the program *PLATON*, and no higher symmetry was found[5]. The detailed crystallographic data for the two compounds were given in Table S1. The bond lengths were listed in Table S2.

Syntheses

$CdPb_8(SeO_3)_4Br_{10}$ was obtained by mild hydrothermal reactions. A mixture of SeO_2 (333 mg, 3 mmol), CdO (128 mg, 1 mmol), $PbBr_2$ (551 mg, 1.5 mmol), 0.25ml HBr and 4 ml H_2O were sealed in an autoclave containing Teflon liner equipped (23 ml), which were heated at 225 °C for 4320 minutes, and then cooled to room temperature at a rate of 1.5 °C/h. The products were separated by vacuum filtration, washed with alcohol and dried in air at room temperature. Transparent crystals $CdPb_8(SeO_3)_4Br_{10}$ was obtained in yield of about 56% (based on Se) respectively. Its purity was confirmed by X-ray diffraction (XRD) and Rietveld refinement (Fig. S1).

$Pb_3(TeO_3)Br_4$ was obtained by mild hydrothermal reactions. A mixture of TeO_2 (479 mg, 3 mmol), $PbBr_2$ (1101 mg, 3 mmol) and 5 ml H_2O were sealed in an autoclave containing Teflon

liner equipped (23 ml), which were heated at 230 °C for 5760 minutes, and then cooled to room temperature at a rate of 3 °C/h. The products were separated by vacuum filtration, washed with alcohol and dried in air at room temperature. Transparent rod-shaped crystals $Pb_3(TeO_3)Br_4$ was obtained in yield of about 11% (based on Se) respectively. Its purity was confirmed by X-ray diffraction (XRD) studies (Fig. S1).

Computational Method

Single-crystal structural data of compounds $CdPb_8(SeO_3)_4Br_{10}$ and $Pb_3(TeO_3)Br_4$ were used for the theoretical calculations. The electronic structures were performed using a plane-wave basis set and pseudo-potentials within density functional theory (DFT) implemented in the total-energy code CASTEP[6]. For the exchange and correlation functional, we chose Perdew–Burke–Ernzerhof (PBE) in the generalized gradient approximation (GGA)[7]. The interactions between the ionic cores and the electrons were described by the ultrasoft pseudopotential[8]. The following valence-electron configurations were considered in the computation: Se-$4s^24p^4$, Te-$5s^25p^4$, Br-$4s^24p^5$, Cd-$4d^{10}4p^25s^2$, Pb-$5d^{10}6p^26s^2$ and O-$2s^22p^4$. The numbers of plane waves included in the basis sets were determined by cutoff energy of 820 eV for $CdPb_8(SeO_3)_4Br_{10}$ and $Pb_3(TeO_3)Br_4$. The numerical integration of the Brillouin zone was performed using Monkhorst-Pack k-point sampling of 1 × 3 × 1 and 3 × 2 × 3. The other parameters and convergent criteria were the default values of CASTEP code.

The calculations of linear optical properties in terms of the complex dielectric function $\varepsilon(\omega) = \varepsilon_1(\omega) + i\varepsilon_2(\omega)$ were made. The imaginary part of the dielectric function ε2 was given in the following equation:

$$\varepsilon^{ij}{}_2(\omega) = \frac{8\pi^2h^2e^2}{(m^2V)}\sum_k\sum_{cv}(f_c - f_v)\frac{p^i_{cv}(k)p^j_{cv}(k)}{E^2_{vc}}\delta[E_c(k) - E_v(k) - h\omega]$$

The f_c and f_v represent the Fermi distribution functions of the conduction and valence band. The term $p^i_{cv}(k)$ denotes the momentum matrix element transition from the energy level c of the conduction band to the level v of the valence band at the *k*th point in the Brillouin zone (BZ), and *V* is the volume of the unit cell[9-11].

The real part $\varepsilon_1(\omega)$ of the dielectric function $\varepsilon(\omega)$ follows from the Kramer–Kronig relationship. All the other optical constants may be derived from $\varepsilon_1(\omega)$ and $\varepsilon_2(\omega)$. For example, the refractive index $n(\omega)$ can be calculated using the following expression[12]:

$$n(\omega)=\left(\frac{1}{\sqrt{2}}\right)\left[\sqrt{\varepsilon_1^2(\omega) + \varepsilon_2^2(\omega)} + \varepsilon_1(\omega)\right]^{1/2}$$

Table S1. Summary of crystal data and structural refinements for $CdPb_8(SeO_3)_4Br_{10}$ and $Pb_3(TeO_3)Br_4$.

molecular formula	**$CdPb_8(SeO_3)_4Br_{10}$**	**$Pb_3(TeO_3)Br_4$**
Formula Weight	3076.86	1116.81
Crystal system	monoclinic	orthorhombic
Space group	*C*2/*c*	*Pna*2$_1$
Temperature(K)	292.31(10)	293(2)
F(000)	5144.0	1848.0
a/Å	17.9188(17)	7.6928(2)
b/Å	9.6194(9)	16.7016(4)
c/Å	17.9097(17)	8.6092(2)
α(deg)	90	90
β(deg)	92.999(9)	90
γ(deg)	90	90
V/Å^3	3082.8(5)	1106.13(5)
Z	4	4
Dc(g.cm^{-3})	6.629	6.706
Flack	/	0.013(12)
GOF on F^2	1.129	1.059
R_1, $wR_2[I > 2\sigma(I)]^a$	$R_1 = 0.0406$, $wR_2 = 0.0790$	$R_1 = 0.0286$, $wR_2 = 0.0696$
R_1, wR_2 (all data)^a	$R_1 = 0.0554$, $wR_2 = 0.0846$	$R_1 = 0.0309$, $wR_2 = 0.0706$
^{a} $R_1 = \sum\|\|F_o\| - \|F_c\|\|/\sum\|F_o\|$, $wR_2 = \{\sum w[(F_o)^2 - (F_c)^2]^2/\sum w[(F_o)^2]^2\}^{1/2}$		

Table S2. Calculated bond valences of the $CdPb_8(SeO_3)_4Br_{10}$ and $Pb_3(TeO_3)Br_4$.

Compound	Bond	Bond lengths	Bond-valence	BVS
$CdPb_8(SeO_3)_4Br_{10}$	Se1-O1	1.702	1.343	3.922
	Se1-O2	1.736	1.225	
	Se1-O3	1.699	1.354	
	Se2-O4	1.692	1.379	4.036
	Se2-O5	1.705	1.332	
	Se2-O6	1.707	1.325	
	Pb1-Br3#1	3.193	0.224	1.492 1.885
	Pb1-O1#2	2.611	0.260	
	Pb1-O1#3	2.659	0.228	
	Pb1-O2#3	2.613	0.258	
	Pb1-O3#2	2.698	0.205	
	Pb1-O4	2.537	0.317	
	Pb1-Br4	3.384	0.134	
	Pb1-Br5	3.347	0.148	
	Pb1-Br5	3.454	0.111	
	Pb2-Br1#4	3.121	0.304	1.515 1.926
	Pb2-O1#2	2.606	0.263	
	Pb2-O4#5	2.694	0.207	
	Pb2-O4	2.641	0.239	
	Pb2-O5	2.660	0.227	
	Pb2-O6#5	2.590	0.275	
	Pb2-Br1	3.35	0.147	
	Pb2-Br2	3.302	0.167	
	Pb2-Br3	3.502	0.097	
	Pb3-Br1	3.106	0.284	2.039
	Pb3-Br2	3.022	0.356	
	Pb3-Br3	3.148	0.253	
	Pb3-Br3#6	3.155	0.249	
	Pb3-Br4	3.113	0.278	
	Pb3-Br5#5	3.162	0.244	
	Pb3-O3	2.729	0.189	
	Pb3-O5	2.734	0.186	
	Pb4-Br1	3.178	0.234	1.553 1.982
	Pb4-Br4#7	3.130	0.266	
	Pb4-Br5	3.067	0.315	
	Pb4-O2	2.534	0.320	
	Pb4-O6#5	2.435	0.418	

	Pb4-Br2	3.404	0.172	
	Pb4-Br2	3.502	0.097	
	Pb4-Br4	3.317	0.160	
	Cd1-O2	2.617	0.146	1.744
	Cd1-O2#5	2.617	0.146	
	Cd1-O3	2.296	0.347	
	Cd1-O3#5	2.296	0.347	
	Cd1-O5	2.263	0.379	
	Cd1-O5#5	2.263	0.379	
$Pb_3(TeO_3)Br_4$	Te1-O1	1.866	1.350	3.984
	Te1-O2	1.891	1.262	
	Te1-O3	1.860	1.372	
	Pb1-Br1	2.942	0.442	1.797 1.967
	Pb1-Br2	3.131	0.265	
	Pb1-Br3#1	3.189	0.227	
	Pb1-O1#1	2.394	0.467	
	Pb1-O2	2.455	0.396	
	Pb1-Br2	3.282	0.176	
	Pb1-Br3	3.297	0.169	
	Pb2-Br2	3.100	0.288	1.844 1.943
	Pb2-Br2#3	3.179	0.233	
	Pb2-Br3#3	3.195	0.223	
	Pb2-Br3	3.161	0.245	
	Pb2-Br4	2.938	0.447	
	Pb2-O3	2.444	0.408	
	Pb2-O2	2.966	0.099	
	Pb3-Br1#4	3.030	0.349	1.640 1.948
	Pb3-Br3#3	3.230	0.203	
	Pb3-O1#4	2.581	0.282	
	Pb3-O2#4	2.543	0.312	
	Pb3-O3	2.373	0.494	
	Pb3-Br4	3.256	0.189	
	Pb3-Br4	3.427	0.119	

Green font: Longer secondary bonds are considered.

Symmetry transformations used to generate equivalent atoms:

For $CdPb_8(SeO_3)_4Br_{10}$: #1 X,1-Y,1/2+Z; #2 +X,1+Y,+Z; #3 1-X,1+Y,3/2-Z; #4 1-X,1-Y,1-Z; #5 1-X,+Y,3/2-Z; #6 3/2-X,1/2-Y,1-Z; #7 -1/2+X,1/2+Y,+Z

For $Pb_3(TeO_3)Br_4$: #1 +X,+Y,-1+Z; #2 1-X,1-Y,-1/2+Z; #3 -1/2+X,1/2-Y,+Z; #4 1-X,1-Y,1/2+Z; #5 +X,+Y,1+Z;#6 1/2+X,1/2-Y,+Z

Table S3. Calculation of the dipole moments of some building blocks in $CdPb_8(SeO_3)_4Br_{10}$ and $Pb_3(TeO_3)Br_4$ (D = Debyes).

$CdPb_8(SeO_3)_4Br_{10}$					
Polar unit		Dipole moment (D)			
Building Blocks	total magnitude	total magnitude	x-component	y-component	z-component
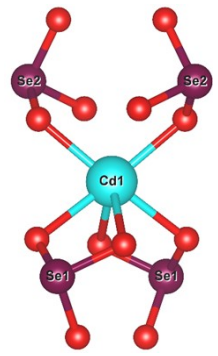	$Se(1)O_3$	10.223	-0.745	0.644	10.176
	$Se(1)O_3$	10.223	0.745	0.644	-10.176
	$Se(2)O_3$	10.414	-10.344	-0.211	1.189
	$Se(2)O_3$	10.414	10.344	-0.211	-1.189
	Net dipole moment of $(SeO_3)_4$	0.866	0	0.866	0
	$Cd(1)O_6$	5.245	0.000	5.245	0.000
	Net dipole moment of $Cd(SeO_3)_4$	3.597	0	3.597	0
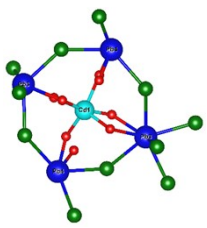	$Cd(1)O_6$	4.379	0.000	4.379	0.000
	$Pb(3)O_2Br_6$	4.417	3.364	-0.757	-2.760
	$Pb(3)O_2Br_6$	4.417	-3.364	-0.757	2.760
	$Pb(4)O_2Br_3$	14.014	3.370	-6.258	12.078
	$Pb(4)O_2Br_3$	14.014	-3.370	-6.259	-12.078
	Net dipole moment of $CdPb_4O_6Br_{14}$	9.652	0.000	-9.652	0.000
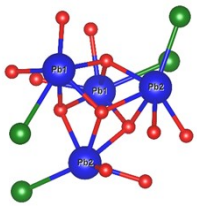	$Pb(1)O_5Br$	13.556	10.066	-2.575	-8.708
	$Pb(1)O_5Br$	13.556	-10.066	-2.575	8.708
	$Pb(2)O_5Br$	4.311	0.377	3.130	-2.941
	$Pb(2)O_5Br$	4.311	-0.377	3.130	2.941
	Net dipole moment of $Pb_4O_{12}Br_4$	6.260	0.000	6.259	0.000
$Pb_3(TeO_3)Br_4$					
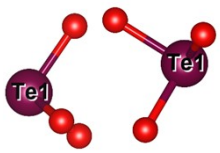	$Te(1)O_3$	11.884	10.499	-0.433	5.550
	$Te(1)O_3$	11.884	-10.499	0.432	5.552
	Net dipole moment of $(TeO_3)_2$	11.10	0	0	11.102
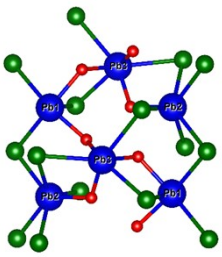	$Pb(1)O_2Br_5$	6.181	-4.857	3.802	-0.391
	$Pb(1)O_2Br_5$	6.181	4.857	-3.802	-0.391
	$Pb(2)OBr_5$	4.703	2.590	-3.913	0.312
	$Pb(2)OBr_5$	4.703	-2.590	3.913	0.312
	$Pb(3)O_3Br_4$	8.052	-0.769	0.667	-7.987
	$Pb(3)O_3Br_4$	8.052	0.769	-0.667	-7.987
	Net dipole moment of this unit	16.133	0	0	-16.133

Table S4. The dipole moments of the polar units and the unit cell of $Pb_3(TeO_3)Cl_4$ and $Pb_3(TeO_3)Br_4$ (D = Debyes).

$Pb_3(TeO_3)Cl_4$				
Polar unit	Dipole moment (D)			
	total magnitude	x-component	y-component	z-component
$Te(1)O_3$	12.833	11.353	0.056	5.982
	12.824	11.344	-0.056	5.981
	12.822	-11.343	0.0564	5.979
	12.832	-11.353	-0.056	5.982
Net dipole moment of $Te(1)O_3$	23.925	0.001	0.001	23.925
$Pb(1)O_3Cl_4$	9.509	-5.089	1.093	-7.957
	9.508	5.089	1.092	-7.957
	9.509	5.089	-1.094	-7.958
	9.509	-5.089	-1.094	-7.958
Net dipole moment of $Pb(1)O_3Cl_4$	31.831	0	-0.003	-31.831
$Pb(2)OCl_5$	2.098	2.097	-0.030	-0.054
	2.098	2.097	0.030	-0.054
	2.098	-2.097	0.030	-0.054
	2.098	-2.097	-0.030	-0.054
Net dipole moment of $Pb(2)OCl_5$	0.218	0	0	-0.218
$Pb(3)O_2Cl_5$	5.135	-4.585	2.308	-0.138
	5.135	-4.585	-2.308	-0.138
	5.136	4.586	-2.308	-0.140
	5.136	4.586	2.308	-0.140
Net dipole moment of $Pb(3)O_2Cl_5$	0.556	0.002	0	-0.556
Net dipole moment (a unit cell)	8.680	-0.418	-0.002	-8.722
$Pb_3(TeO_3)Br_4$				
Polar unit	Dipole moment (D)			
	total magnitude	x-component	y-component	z-component
$Te(1)O_3$	11.888	10.503	0.431	5.552
	11.884	10.499	-0.433	5.550
	11.884	-10.499	0.432	5.552
	11.889	-10.503	-0.431	5.554
Net dipole moment of $Te(1)O_3$	22.208	0	0	22.208
$Pb(1)O_2Br_5$	6.181	4.857	3.802	-0.391
	6.181	4.857	-3.802	-0.391
	6.181	-4.857	3.802	-0.391
	6.181	-4.857	-3.802	-0.391
Net dipole moment of $Pb(1)O_2Br_5$	1.565	0	0	-1.565
$Pb(2)OBr_5$	4.701	2.590	3.911	0.312
	4.701	2.590	-3.911	0.312

	4.701	-2.590	3.911	0.312
	4.701	-2.590	-3.911	0.312
Net dipole moment of $Pb(2)OBr_5$	1.248	0	0	1.248
$Pb(3)O_3Br_4$	8.053	-0.772	-0.665	-7.988
	8.053	-0.772	0.665	-7.988
	8.053	0.772	-0.665	-7.988
	8.053	0.772	0.665	-7.988
Net dipole moment of $Pb(3)O_3Br_4$	32.271	0	0	-32.271
Net dipole moment (a unit cell)	10.062	0	0	-10.062

Table S5. State energies (eV) of the lowest conduction band (L-CB) and the highest valence band (H-VB) of $CdPb_8(SeO_3)_4Br_{10}$ and $Pb_3(TeO_3)Br_4$.

Compound	k-point	L-CB	H-VB
$CdPb_8(SeO_3)_4Br_{10}$	Z (0.000, 0.000, 0.500)	3.011678	-0.18565
	G (0.000, 0.000, 0.000)	2.954599	-0.15266
	Y (0.000, 0.500, 0.000)	2.967506	-0.00769
	A (-0.500, 0.500, 0.000)	3.129502	-0.00064
	B (-0.500, 0.000, 0.000)	3.058268	-0.21462
	D (-0.500, 0.000, 0.500)	3.045194	-0.24492
	E (-0.500, 0.500, 0.500)	3.083478	0
	C (0.000, 0.500, 0.500)	3.133588	-0.03147
$Pb_3(TeO_3)Br_4$	G (0.000, 0.000, 0.000)	3.134203	0
	Z (0.000, 0.000, 0.500)	3.401155	-0.11537
	T (-0.500, 0.000, 0.500)	3.298867	-0.11899
	Y (-0.500, 0.000, 0.000)	3.458111	-0.02856
	S (-0.500, 0.500, 0.000)	3.532037	-0.0913
	X (0.000, 0.500, 0.000)	3.149716	-0.04157
	U (0.000, 0.500, 0.500)	3.438794	-0.11292
	R (-0.500, 0.500, 0.500)	3.295515	-0.07356

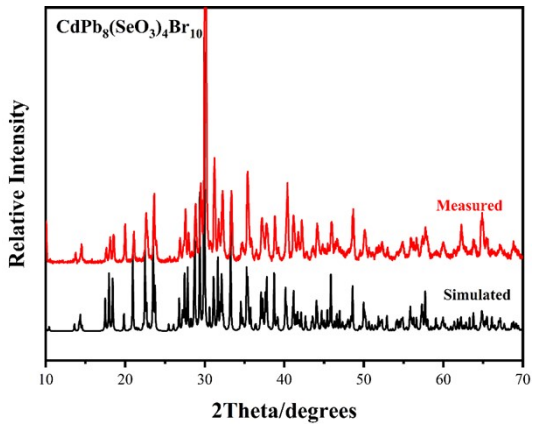

(a)

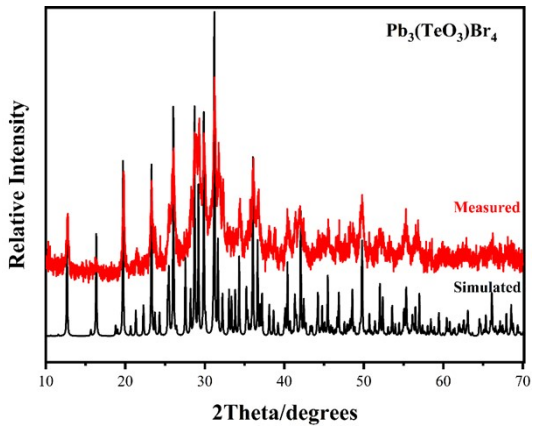

(b)

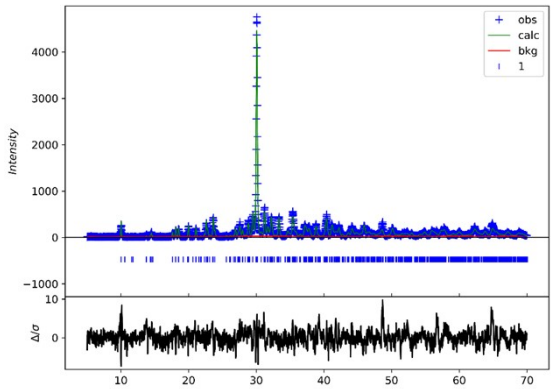

(c)

Figure S1. Simulated and experimental powder X-ray diffractometer patterns of $CdPb_8(SeO_3)_4Br_{10}$ (a),$Pb_3(TeO_3)Br_4$ (b) and Rietveld refinement plots of the powder XRD patterns for $CdPb_8(SeO_3)_4Br_{10}$ (c).

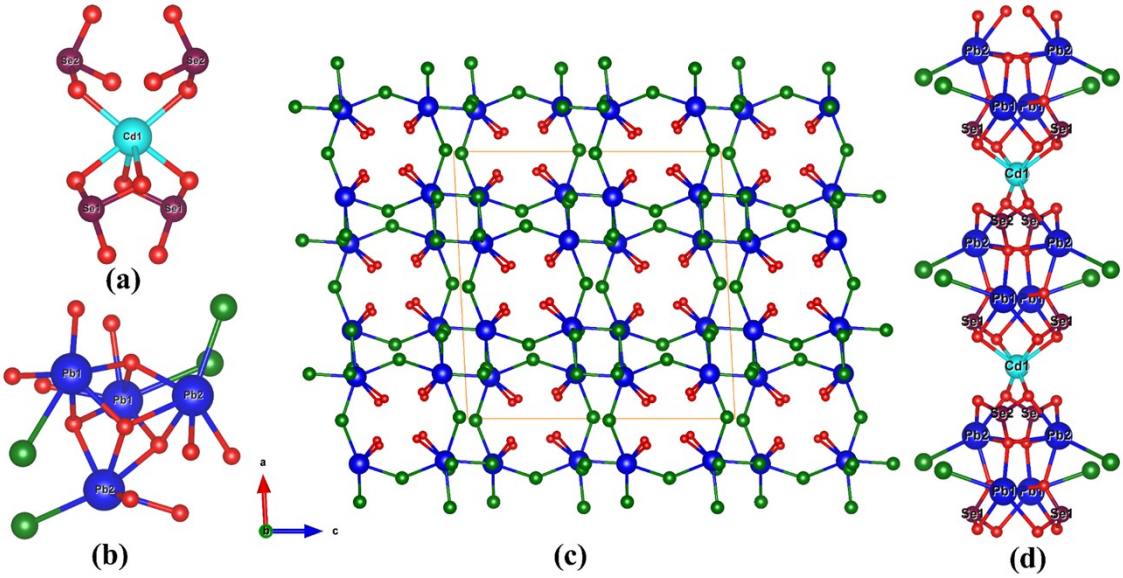

Figure S2. The $[Cd(SeO_3)_4]^{6-}$ unit (a), $Pb_4O_{12}Br_4$ tetramers (b), 3D network with four-membered polyhedral ring (4-MR) tunnels (c) and the 1D chain formed by the $[Cd(SeO_3)_4]^{6-}$ units and $Pb_4O_{12}Br_4$ tetramers(d).

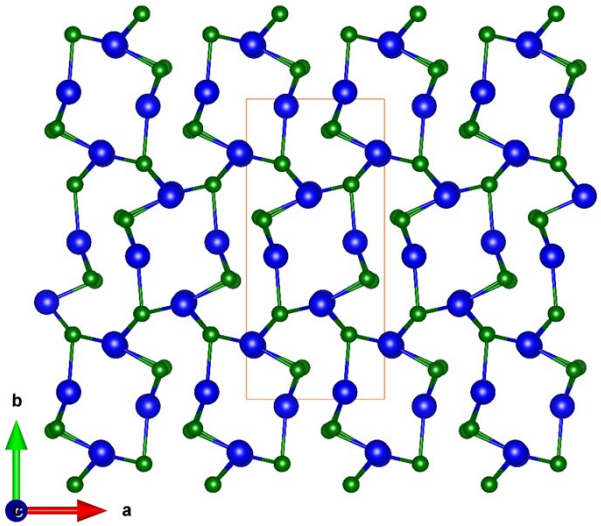

(a)

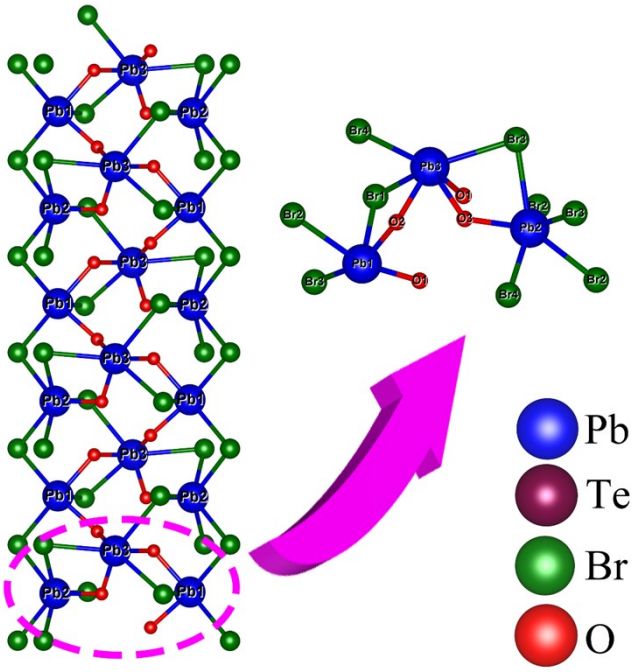

(b)

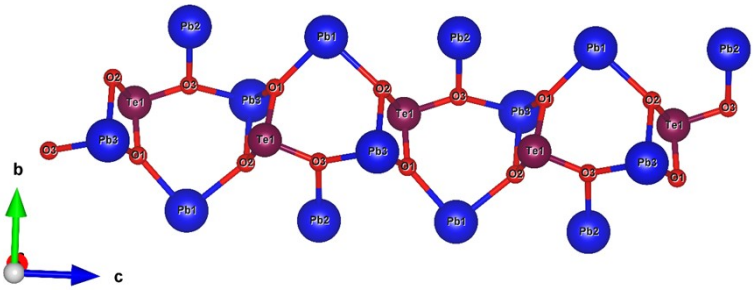

(c)

Figure S3. The lead bromide 3D skeletons (a), the 1D lead bromoxide 4-MR structures (b) and the lead tellurite chain (c) of $Pb_3(TeO_3)Br_4$.

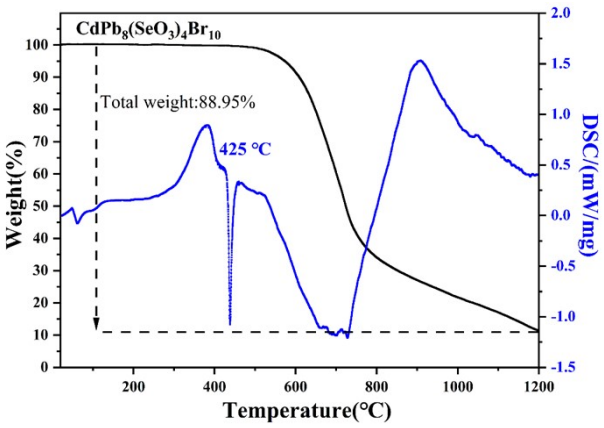

(a)

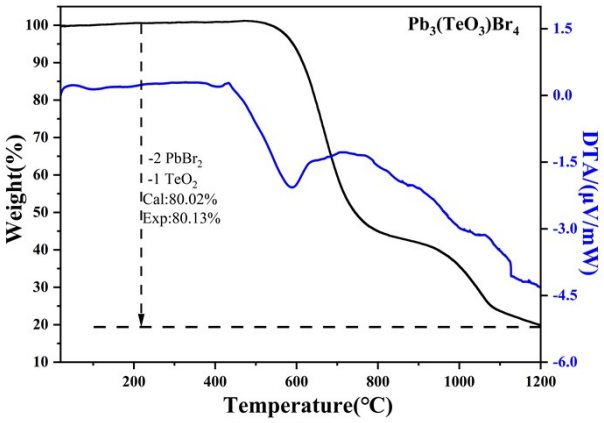

(b)

Figure S4. TGA and DSC/DTA results of $CdPb_8(SeO_3)_4Br_{10}$ (a) and $Pb_3(TeO_3)Br_4$ (b).

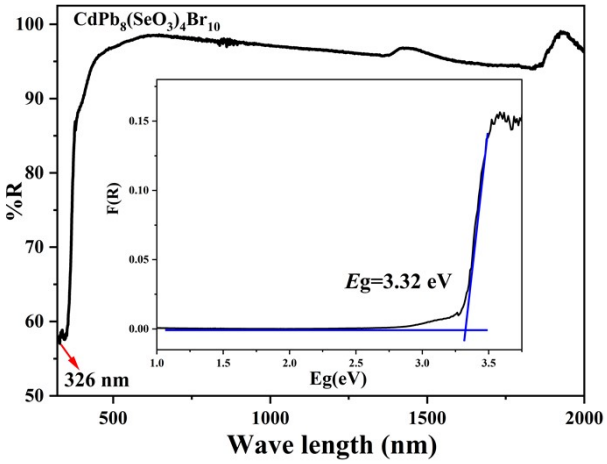

(a)

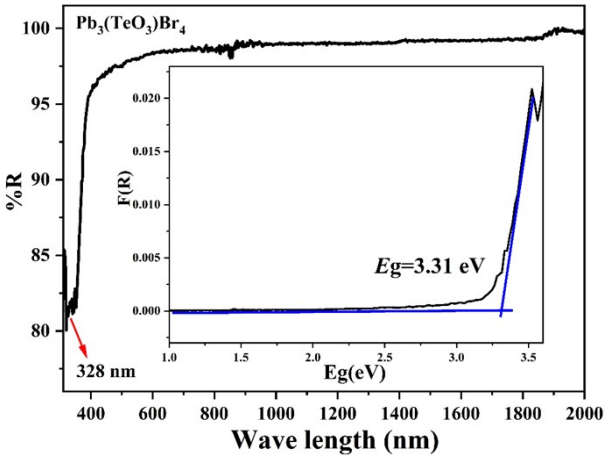

(b)

Figure S5. UV−vis−NIR diffuse-reflectance spectra of $CdPb_8(SeO_3)_4Br_{10}$ (a) and $Pb_3(TeO_3)Br_4$ (b).

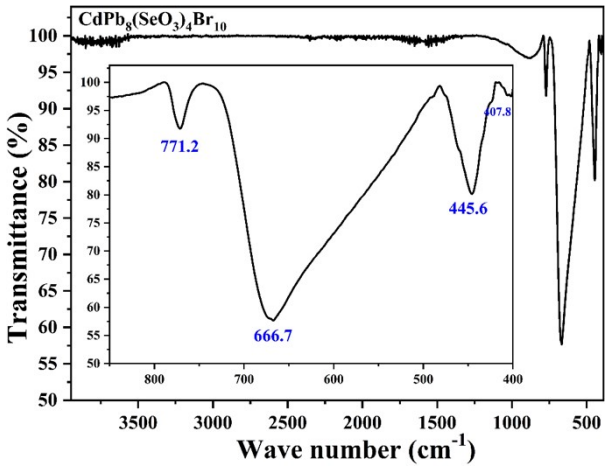

(a)

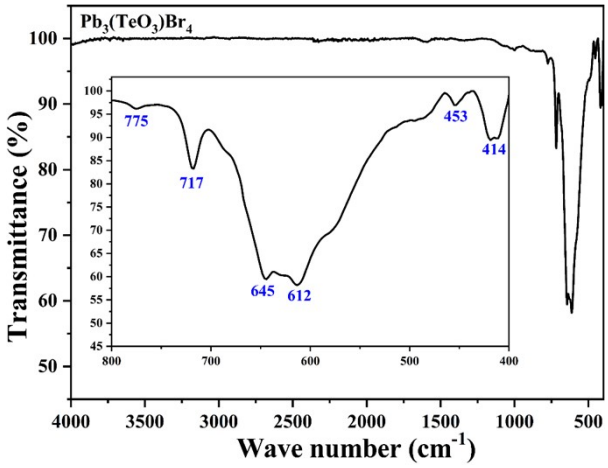

(b)

Figure S6. IR spectra of $CdPb_8(SeO_3)_4Br_{10}$ (a) and $Pb_3(TeO_3)Br_4$ (b).

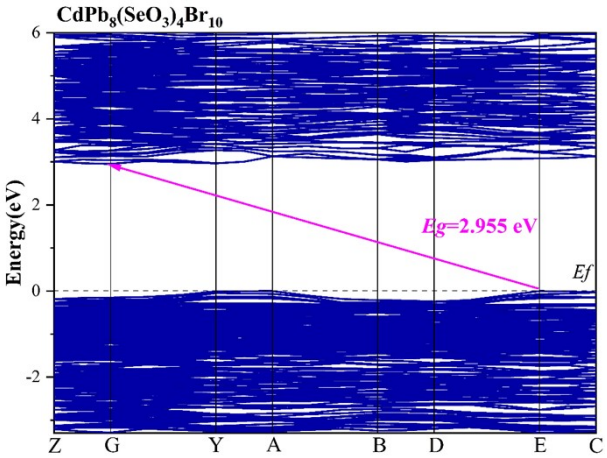

(a)

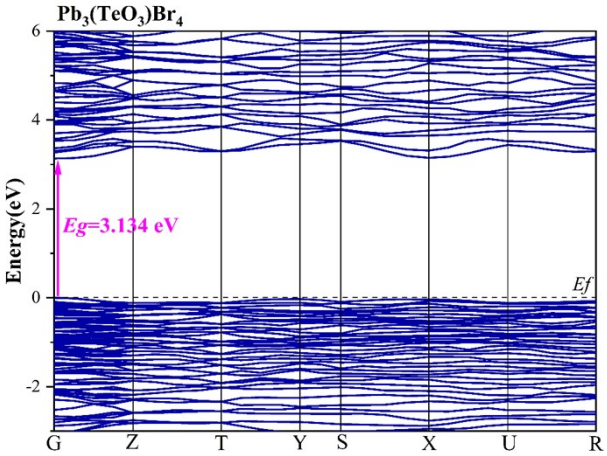

(b)

Figure S7. Band structures of $CdPb_8(SeO_3)_4Br_{10}$ (a) and $Pb_3(TeO_3)Br_4$ (b).

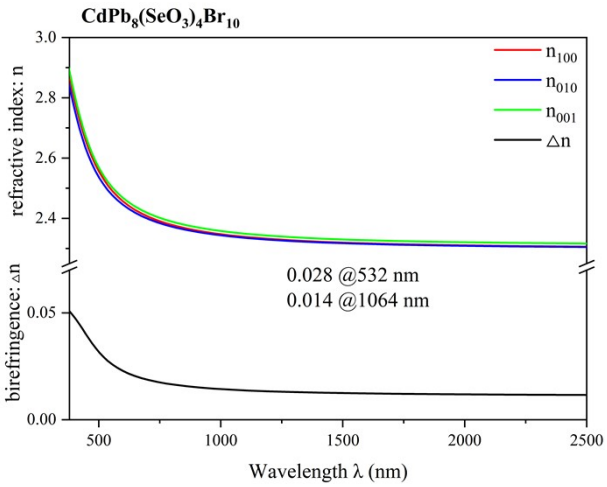

Figure S8. Calculated refractive indices and birefringence of $CdPb_8(SeO_3)_4Br_{10}$ (a).

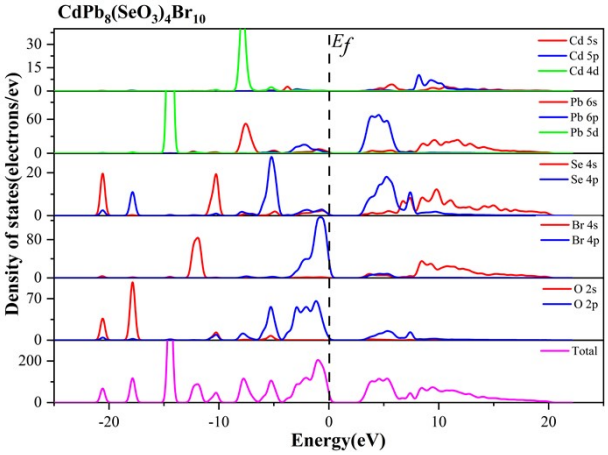

Figure S9. Total and partial density of states of $CdPb_8(SeO_3)_4Br_{10}$.

References

1. P. Kubelka and F. Munk, An Article on Optics of Paint Layers, *Technol. Physical* 1931, **12**, 259−274.
2. S. K. Kurtz and T. T. Perry, A Powder Technique for the Evaluation of Nonlinear Optical Materials., *J. Appl. Phys.*, 1968, **39**, 3798-3813.
3. O. V. Dolomanov, L. J. Bourhis, R. J. Gildea, J. A. K. Howard and H. Puschmann, OLEX2: a complete structure solution, refinement and analysis program, *J. Appl. Cryst.*, 2009, **42**, 339-341.
4. G. M. Sheldrick, Crystal structure refinement with SHELXL, *Acta Cryst.*, 2015, **C71**, 3-8.
5. A. L. Spek, Single-crystal structure validation with the program PLATON, *J. Appl. Cryst.*, 2003, **36**, 7−13.
6. M. D. Segall, P. J. D. Lindan, M. J. Probert, C. J. Pickard, P. J. Hasnip, S. J. Clark and M. C. Payne, First-principles simulation: ideas, illustrations and the CASTEP code, *Phys-Condens Mat.*, 2002, **14**, 2717-2744.
7. V. Milman, B. Winkler, J. A. White, C. J. Pickard, M. C. Payne, E. V. Akhmatskaya and R. H. Nobes, Electronic structure, properties, and phase stability of inorganic crystals: A pseudopotential plane-wave study, *Int. J. Quantum. Chem.*, 2000, **77**, 895-910.
8. J. P. Perdew, K. Burke and M. Ernzerhof, Generalized Gradient Approximation Made Simple, *Phys. Rev. Lett.*, 1996, **77**, 3865-3868.
9. C. Aversa and J. E. Sipe, Nonlinear optical susceptibilities of semiconductors: Results with a length-gauge analysis, *Phys. Rev. B*, 1995, **52**, 14636-14645.
10. J. Lin, M.-H. Lee, Z.-P. Liu, C. Chen and C. J. Pickard, Mechanism for linear and nonlinear optical effects in$\beta-BaB_2O_4$ crystals, *Phys. Rev. B*, 1999, **60**, 13380-13389.
11. S. N. Rashkeev, W. R. L. Lambrecht and B. Segall, Efficientab initiomethod for the calculation of frequency-dependent second-order optical response in semiconductors, *Phys. Rev. B*, 1998, **57**, 3905-3919.
12. D. Vanderbilt, Soft self-consistent pseudopotentials in a generalized eigenvalue formalism, *Phys. Rev. B*, 1990, **41**, 7892-7895.